JOURNAL OF COMPUTATIONAL PHYSICS 8, 119–143 (1971)

A Computing Method for Incompressible Flows Bounded by Moving Walls*

JAMES A. VIECELLI

Lawrence Radiation Laboratory, University of California, Livermore, California 94550

Received November 16, 1970

A modified type of Marker and Cell computing method is presented for solving problems in incompressible hydrodynamics. The method is applicable to time dependent problems in two spatial dimensions or three spatial dimensions with axial symmetry. Details are presented for calculation of arbitrarily shaped curved wall boundaries and flexible moving wall boundaries. Example problems with moving walls and free surfaces are given.

INTRODUCTION

The MAC or Marker and Cell method is a technique for solving the time dependent Eulerian equations of incompressible hydrodynamics and is especially suited for flows containing free surfaces [1]. The method is based on representing the time dependent partial differential equations of momentum conservation by finite differences over a rectangular net of points. Substitution of the resulting expressions for the time advanced u and v components of velocity into a finite difference form of the continuity equation yields a finite difference approximation to a Poisson equation for the pressure. The solution is advanced in time by a series of repeated steps. First one solves the Poisson equation for the pressure which is then used in the momentum equations to calculate new velocity components. A new source term for the Poisson equation is calculated from the new velocity field and the cycle begins over again. Marker particles, moved with velocities interpolated from the Eulerian mesh point values, allow one to tell which of the rectangular finite difference cells contain free surface boundaries. The method has been used to compute wave motion, Taylor instability, and the splash of a liquid drop [2–4]. However engineering applications have been limited by the requirement that external wall shapes be confined to fixed rectangular segments of the Eulerian mesh.

Recently, the limitation on wall boundary shapes has been overcome by treating

* This work was performed under the auspices of the U. S. Atomic Energy Commission.

free slip rigid wall boundaries as if they were free surfaces with a pressure distribution applied in such a way that the free surface position coincides with the wall boundary [5]. To this end the usual iterative solution of the Poisson equation, followed by computation of new velocities, is replaced by an iteration method in which both the velocity and pressure are adjusted simultaneously. A special iteration formula for the pressure in free surface curved-wall boundary cells then permits calculation of the pressure distribution. This method of treating curved wall boundaries can be extended to include moving walls so that it is possible to calculate flows over objects that undergo large deformations or move about the mesh. This report gives more details of the arbitrary boundary method (ABMAC), some improvements, and the changes required for moving boundaries.

Simultaneous Iteration Methods

The dependent variables are u the radial component of the velocity, spatially centered at $(k+\frac{1}{2}, l)$, v the axial component of the velocity centered at $(k, l+\frac{1}{2})$, and P the pressure, centered at (k, l). There are many ways of differencing the equations for the components of the momentum. ABMAC includes an option for selecting either backward or centered spatial differencing in the advection terms. With time derivatives approximated by simple forward differences and spatial derivatives by centered differences the finite difference representation of the u component momentum equation is

$$u^{n+1}_{k+\frac{1}{2},l} = u^n_{k+\frac{1}{2},l} - \frac{\Delta t}{r^\alpha \Delta r}[(r^\alpha u^2)^n_{k+1,l} - (r^\alpha u^2)^n_{k,l}] - \frac{\Delta t}{\rho \Delta r}[P_{k+1,l} - P_{k,l}]$$

$$- \frac{\Delta t}{\Delta z}[(vu)^n_{k+\frac{1}{2},l+\frac{1}{2}} - (vu)^n_{k+\frac{1}{2},l-\frac{1}{2}}] - g_r \Delta t$$

$$+ \frac{\nu \Delta t}{\Delta z^2}[u^n_{k+\frac{1}{2},l+1} - 2u^n_{k+\frac{1}{2},l} + u^n_{k+\frac{1}{2},l-1}]$$

$$- \nu \frac{\Delta t}{\Delta r \Delta z}[v^n_{k+1,l+\frac{1}{2}} - v^n_{k+1,l-\frac{1}{2}} - v^n_{k,l+\frac{1}{2}} + v^n_{k,l-\frac{1}{2}}] \tag{1a}$$

The old velocity, advection, body force, and viscous terms can be grouped together to give

$$u^{n+1}_{k+\frac{1}{2},l} = \eta^n_{k+\frac{1}{2},l} - \frac{\Delta t}{\rho \Delta r}[P_{k+1,l} - P_{k,l}]. \tag{1b}$$

The centered difference form for the v component is

$$v^{n+1}_{k,l+\frac{1}{2}} = v^n_{k,l+\frac{1}{2}} - \frac{\Delta t}{\Delta z}[(v^2)^n_{k,l+1} - (v^2)^n_{k,l}] - \frac{\Delta t}{\rho\,\Delta z}[P_{k,l+1} - P_{k,l}]$$
$$- \frac{\Delta t}{r^\alpha\,\Delta r}[(r^\alpha uv)^n_{k+\frac{1}{2},l+\frac{1}{2}} - (r^\alpha uv)^n_{k-\frac{1}{2},l+\frac{1}{2}}] - g_z\,\Delta t$$
$$- \frac{\nu\,\Delta t}{r^\alpha\,\Delta r\,\Delta z}[(u^n_{k+\frac{1}{2},l+1} - u^n_{k+\frac{1}{2},l})\,r^\alpha_{k+\frac{1}{2}} - (u^n_{k-\frac{1}{2},l+1} - u^n_{k-\frac{1}{2},l})\,r^\alpha_{k-\frac{1}{2}}]$$
$$- \frac{\nu\,\Delta t}{r^\alpha\,\Delta r^2}[(v^n_{k,l+\frac{1}{2}} - v^n_{k-1,l+\frac{1}{2}})\,r^\alpha_{k-\frac{1}{2}} - (v^n_{k+1,l+\frac{1}{2}} - v^n_{k,l+\frac{1}{2}})\,r^\alpha_{k+\frac{1}{2}}], \qquad (2a)$$

which can be written

$$v^{n+1}_{k,l+\frac{1}{2}} = \xi^n_{k,l+\frac{1}{2}} - \frac{\Delta t}{\rho\,\Delta z}[P_{k,l+1} - P_{k,l}]. \qquad (2b)$$

For slab geometry $\alpha = 0$ and for cylindrical symmetry $\alpha = 1$. Quantities not directly available such as $u_{k+1,l}$ are obtained by simple averaging. In the backwards difference formulation of the advection terms one would, for example, replace

$$[(r^\alpha u^2)^n_{k+1,l} - (r^\alpha u^2)^n_{k,l}]$$

in the u component equation by

$$\left[r^\alpha u^n_{k+1,l}\begin{cases} u^n_{k+\frac{3}{2},l} & \text{if} \quad u^n_{k+1,l} < 0 \\ u^n_{k+\frac{1}{2},l} & \text{if} \quad u^n_{k+1,l} > 0 \end{cases} - r^\alpha u^n_{k,l}\begin{cases} u^n_{k+\frac{1}{2},l} & \text{if} \quad u^n_{k,l} < 0 \\ u_{k-\frac{1}{2},l} & \text{if} \quad u^n_{k,l} > 0 \end{cases}\right]$$

and

$$[(vu)^n_{k+\frac{1}{2},l+\frac{1}{2}} - (vu)^n_{k+\frac{1}{2},l-\frac{1}{2}}]$$

would be replaced by

$$\left[v^n_{k+\frac{1}{2},l+\frac{1}{2}}\begin{cases} u^n_{k+\frac{1}{2},l+1} & \text{if} \quad v^n_{k+\frac{1}{2},l+\frac{1}{2}} < 0 \\ u^n_{k+\frac{1}{2},l} & \text{if} \quad v^n_{k+\frac{1}{2},l+\frac{1}{2}} > 0 \end{cases} - v^n_{k+\frac{1}{2},l-\frac{1}{2}}\begin{cases} u^n_{k+\frac{1}{2},l} & \text{if} \quad v^n_{k+\frac{1}{2},l-\frac{1}{2}} < 0 \\ u^n_{k+\frac{1}{2},l-1} & \text{if} \quad v^n_{k+\frac{1}{2},l-\frac{1}{2}} > 0 \end{cases}\right].$$

Similarly in the v component equation the backwards difference formulation of the advection terms would require replacement of

$$[(v^2)^n_{k,l+1} - (v^2)^n_{k,l}]$$

by

$$\left[v^n_{k,l+1}\begin{Bmatrix} v^n_{k,l+\frac{1}{2}} & \text{if} & v^n_{k,l+1} > 0 \\ v^n_{k,l+\frac{3}{2}} & \text{if} & v^n_{k,l+1} < 0 \end{Bmatrix} - v^n_{k,l}\begin{Bmatrix} v^n_{k,l+\frac{1}{2}} & \text{if} & v^n_{k,l} < 0 \\ v^n_{k,l-\frac{1}{2}} & \text{if} & v^n_{k,l} > 0 \end{Bmatrix}\right]$$

and

$$[(r^\alpha uv)^n_{k+\frac{1}{2},l+\frac{1}{2}} - (r^\alpha uv)^n_{k-\frac{1}{2},l+\frac{1}{2}}]$$

by

$$\left[(r^\alpha u)^n_{k+\frac{1}{2},l+\frac{1}{2}}\begin{Bmatrix} v^n_{k+1,l+\frac{1}{2}} & \text{if } u^n_{k+\frac{1}{2},l+\frac{1}{2}} < 0 \\ v^n_{k,l+\frac{1}{2}} & \text{if } u^n_{k+\frac{1}{2},l+\frac{1}{2}} > 0 \end{Bmatrix} - (r^\alpha u)^n_{k-\frac{1}{2},l+\frac{1}{2}}\begin{Bmatrix} v^n_{k,l+\frac{1}{2}} & \text{if } u^n_{k-\frac{1}{2},l+\frac{1}{2}} < 0 \\ v^n_{k-1,l+\frac{1}{2}} & \text{if } u^n_{k-\frac{1}{2},l+\frac{1}{2}} > 0 \end{Bmatrix}\right]$$

The pressure field $P_{k,l}$ is to be determined such that the advanced time velocity components $u^{n+1}_{k+\frac{1}{2},l}$ and $v^{n+1}_{k,l+\frac{1}{2}}$ obtained from (1b) and (2b) satisfy the continuity equation

$$(\nabla \cdot \mathbf{V})^{n+1}_{k,l} = \frac{1}{\Delta z}[v^{n+1}_{k,l+\frac{1}{2}} - v^{n+1}_{k,l-\frac{1}{2}}] + \frac{1}{r^\alpha \Delta r}[(r^\alpha u)^{n+1}_{k+\frac{1}{2},l} - (r^\alpha u)^{n+1}_{k-\frac{1}{2},l}] = 0. \quad (3)$$

The pressure and the advanced time velocity fields may be solved for simultaneously by introducing the relaxation parameter $\Delta\tau$ and the following iteration formula for the $i+1$ iteration value of the pressure field [6]

$$P^{i+1}_{k,l} = P^i_{k,l} - \Delta\tau(\nabla \cdot \mathbf{V}^{n+1})^i_{k,l}\,. \quad (4)$$

One method of iteration is: (a) use Eq. (4) to compute a new pressure field; (b) substitute the new pressure field into Eqs. (1b) and (2b) and compute values for $(u^{n+1}_{k+\frac{1}{2},l})^{i+1}$ and $(v^{n+1}_{k,l+\frac{1}{2}})^{i+1}$; (c) use the new velocities to compute new values of the divergence, $(\nabla \cdot \mathbf{v}^{n+1})^{i+1}_{k,l}$. Continue repeating these three steps until changes in the iterates $P^i_{k,l}$, $(u^{n+1}_{k+\frac{1}{2},l})^i$ and $(v^{n+1}_{k,l+\frac{1}{2}})^i$ fall below some small error limit. To save time do not recompute the advection and viscous terms at each cycle of iteration, but instead store them in the variables $\eta^n_{k+\frac{1}{2},l}$ and $\xi^n_{k,l+\frac{1}{2}}$.

The nature of the iteration can be made clearer by substituting Eqs. (1b) and (2b) with $P_{k,l} = P^i_{k,l}$ into (3) and then substituting the result into (4). For the case $\alpha = 0$, $\Delta r = \Delta z = \delta$ one obtains

$$P^{i+1}_{k,l} = P^i_{k,l} + \frac{\Delta\tau\,\Delta t}{\rho\delta^2}[P^i_{k+1,l} + P^i_{k-1,l} + P^i_{k,l+1} + P^i_{k,l-1} - 4P^i_{k,l}] - \Delta\tau\, S_{k,l}\,, \quad (5)$$

where $S_{k,l}$ is a source function of the variables $\eta^n_{k+\frac{1}{2},l}$ and $\xi^n_{k,l+\frac{1}{2}}$. This is the difference equation one effectively solves when one adjusts all of the mesh pressures

before computing any new velocities. It is clear that it is just a finite difference representation of the partial differential equation

$$\frac{\partial P}{\partial \tau} = \sigma \nabla^2 P - S, \qquad \sigma = \Delta t/\rho. \tag{6}$$

By continued iteration one approaches the asymptotic solution which is

$$\nabla^2 P = S/\sigma. \tag{7}$$

Upon expanding S in terms of the mesh values of u and v contained in the η and ξ temporary storage variables one would find that (7) is the usual Poisson equation for the pressure, including the divergence correction term for the error in the velocity at time $n\Delta t$.

A von Neumann Fourier analysis [7] of (5) shows that one must choose $\Delta\tau \leqslant \rho\delta^2/4\Delta t$, otherwise numerical instability will occur. It is important to note that the asymptotic approach of the diffusion equation (6) to the steady state is slow and that the simple relaxation equation (5) is very inefficient because of the restriction on the size of $\Delta\tau$. A very much improved formula, equivalent to successive over relaxation, is obtained by replacing $P^i_{k-1,l}$ and $P^i_{k,l-1}$ with the latest iterates $P^{i+1}_{k-1,l}$ and $P^{i+1}_{k,l-1}$ while sweeping in the direction of increasing k and l. This yields

$$P^{i+1}_{k,l} = P^i_{k,l} + \frac{\Delta\tau\,\Delta t}{\rho\delta^2}\left[P^i_{k+1,l} + P^{i+1}_{k-1,l} + P^i_{k,l+1} + P^{i+1}_{k,l-1} - 4P^i_{k,l}\right] - \Delta\tau\, S_{k,l}\,. \tag{8}$$

A Von Neumann analysis of this equation yields the stability restriction $\Delta\tau \leqslant \rho\delta^2/2\Delta t$. The "time step," $\Delta\tau$, can be made larger and also the equation has more damping than (5) so that the approach to the steady state is much quicker. In order to generate form (8) one must compute new iterates

$$(u^{n+1}_{k+\frac{1}{2},l})^{i+1}, \qquad (u^{n+1}_{k-\frac{1}{2},l})^{i+1}, \qquad (v^{n+1}_{k,l+\frac{1}{2}})^{i+1} \qquad \text{and} \qquad (v^{n+1}_{k,l-\frac{1}{2}})^{i+1}$$

a soon as one obtains $P^{i+1}_{k,l}$ for a cell and before advancing to the next cell. Thus if one advances successively in the order of increasing k and increasing l, as indicated by the numbering of the cells in the example in Fig. 1, then the divergence used in calculating a new pressure iterate in cell (k, l) will be based on velocities calculated with new pressure iterates in cells $(k-1, l)$ and $(k, l-1)$ and old pressure iterates in cells (k, l), $(k+1, l)$ and $(k, l+1)$. Hence scheme (8) results.

Sufficient accuracy is normally obtained if the iteration is continued until the ratio of the norm of the pressure changes to the norm of the pressures drops below .0008. For any particular set of boundary conditions there is an optimum value of $\Delta\tau$ for most rapid convergence. In very simple cases this value can be

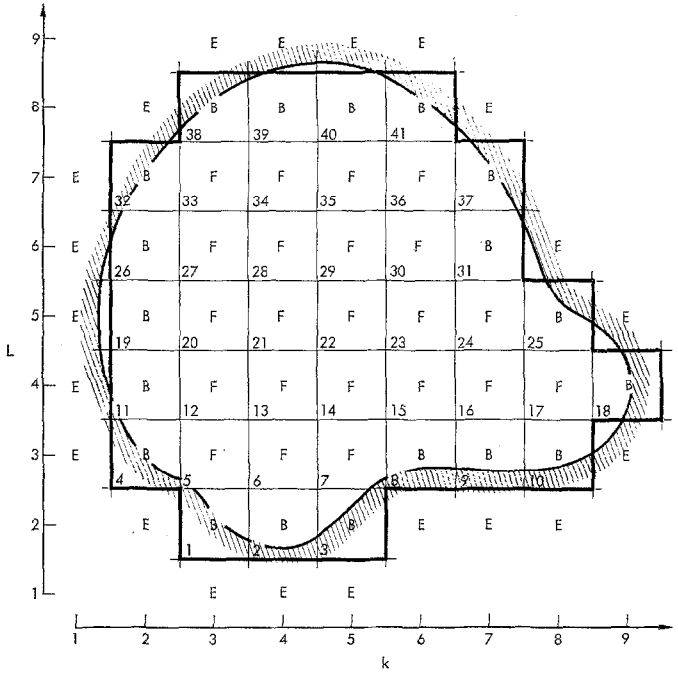

FIG. 1. Cell flags and order of calculation.

computed theoretically but in most computations this is impractical. However, it is usually safe to assume that the optimum value occurs fairly close to the stability limit and to start calculations with $\Delta\tau$ at about $.9\Delta\tau_{\max}$.

FLEXIBLE CURVED WALL BOUNDARIES

In the case of free-slip boundary conditions the motion of an interface between a liquid and a flexible curved wall is equivalent to that of a free surface with an applied pressure distribution. Given any interfacial shape or motion one can produce that same shape or motion with some unique pressure distribution applied to a free surface. This is the basis for ABMAC boundary calculations. Since the MAC method already has a well developed technique for treating free surfaces it is only necessary that one find a way of relating the required pressure distribution to the motion and shape of the boundary.

A moving flexible curved wall can be specified by a locus of points. These points might be the edge intersection points of a Lagrangian mesh covering the wall or body. For example one might be solving the equations of elasticity for the wall

deformations produced by the liquid pressure. Or the points might be given by some prescribed analytic formula for the boundary shape and motion. In general the points will not lie on any of the Eulerian mesh lines used in the finite difference solution of the hydrodynamic equations. The first step is to connect successive points with straight lines and find all of the intersections of these line segments with the underlying Eulerian mesh. One can then represent the boundary section lying inside an Eulerian cell by a single straight line connecting the points of intersection of the boundary with the sides of the cell. Now of course it is possible to think of all sorts of situations where the boundary wanders in and out of a single cell creating some ambiguity. However this occurs only when there are an insufficient number of zones to accurately calculate details of the flow. Therefore it is assumed that the Eulerian zoning is always fine enough so that the boundary has only two intersections with each cell. Having broken the boundary into a set of straight line segments, each associated with a unique Eulerian cell, one can specify the position of each segment by a unit vector normal to the boundary with base positioned at the midpoint of the segment. ABMAC uses the convention that the normal points towards the liquid and to the left as one advances from the ith to $i + 1$th boundary point. Since the boundary may be moving it is also necessary to assign a velocity vector to the midpoint of the segment. If the boundary is part of a Lagrangian mesh one can calculate this velocity by linear interpolation from the values given at the corners of the Lagrangian mesh. Or the velocity may be specified by some input formula as a function of time and distance along the boundary.

The second step is to find a good approximation to the boundary shape using segments of the Eulerian mesh and to define and flag Eulerian boundary cells as those along the inside edges of this approximate contour. This is not actually a very difficult computational task. With the normal convention decided upon one can easily calculate the liquid area of the boundary cells; then if the liquid fraction of the total cell area is greater than a set fraction, usually 1/4, the boundary cell flag is turned on. If the liquid area fraction is too small one can determine which of the four neighboring cells the boundary segment normal points nearest to and then set the boundary flag for that cell. When that cell also contains a boundary segment the two segments can be replaced with one by removing the boundary intersection point between the two adjoining cells. This new segment, spanning two cells, is also defined by velocity and position vectors at its midpoint. Note that as a result of this selection process the midpoint of a boundary segment may not lie in the Eulerian boundary cell it is associated with. Thus it is sometimes necessary to assign a pointer to a boundary cell indicating which neighboring cell contains the midpoint of the associated boundary segment. Once the boundary cell flags have been set it is necessary to go through them and turn off the boundary flag in any cell in the corner of a right angle cell pattern, since such cells are bounded on two adjacent sides by either a pair of interior or exterior cells and on the other

two by boundary cells. Figure 1 shows a closed boundary curve, the approximate Eulerian boundary, and the cell flag pattern. It illustrates the various cases mentioned above. This process of defining a set of Eulerian boundary cells is analogous to the defining of a set of free surface cells in the MAC method but with the additional constraint that the resulting cell pattern avoid overdeterming the boundary condition on the pressure. Cells outside the Eulerian boundary are flagged as exterior cells so that one can tell when velocity components lie on the exterior sides of boundary cells.

When the boundary is stationary the normals and Eulerian cell flags need to be determined only once at the beginning of the calculation; however when the boundary is moving it is necessary to regenerate the normals and cell flags each

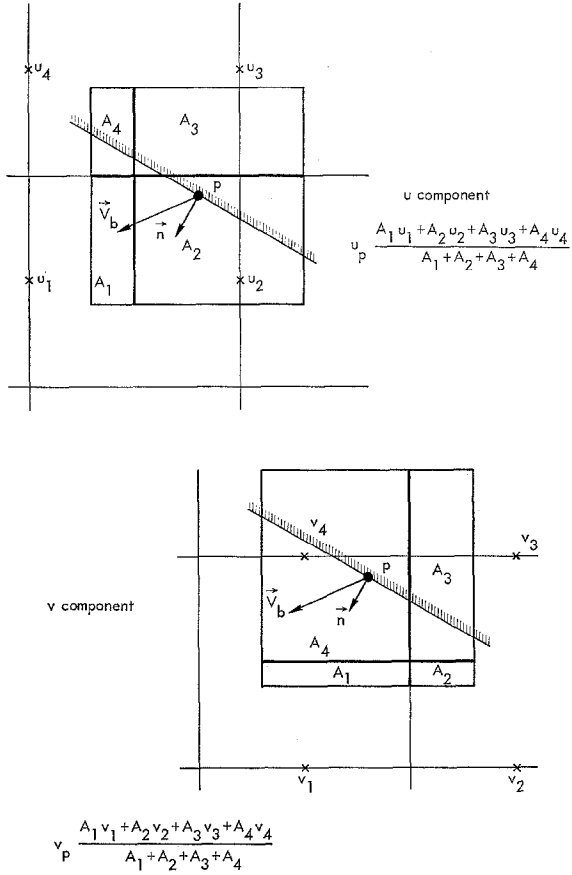

FIG. 2. Interpolating scheme for obtaining the liquid velocity at the midpoint of a boundary segment.

time the solution is advanced Δt in time. The change in position of the Lagrange line defining the boundary, over the time interval Δt, is obtained by multiplying the boundary velocity $\mathbf{V}_b(\mathbf{r}, t)$ at the given point by Δt.

Once the boundary cells have been determined the following relaxation equation is used to compute the pressure in these cells.

$$P_{k,l}^{i+1} = P_{k,l}^{i} - \frac{\Delta\tau}{\delta}\{[(\mathbf{V}_p^{n+1})^i - \mathbf{V}_b(\mathbf{r}, t)] \cdot \mathbf{n}\}_{k,l} . \tag{9}$$

In this equation $\mathbf{n}$ is the normal defining the boundary segment associated with cell (k, l), $(\mathbf{V}_b(\mathbf{r}, t))_{k,l}$ is the velocity of the midpoint of the segment, and $(\mathbf{V}_p^{n+1})^i$ is the liquid velocity at the midpoint of the segment computed with the MAC area weighted interpolation formula as shown in Fig. 2. Clearly $(\mathbf{V}_p^{n+1})_{k,l}^i$ is one of the iterates and must be recomputed each time the pressures and velocities are adjusted. The relaxation parameter and mesh width are $\Delta\tau$, and δ, respectively. The formula

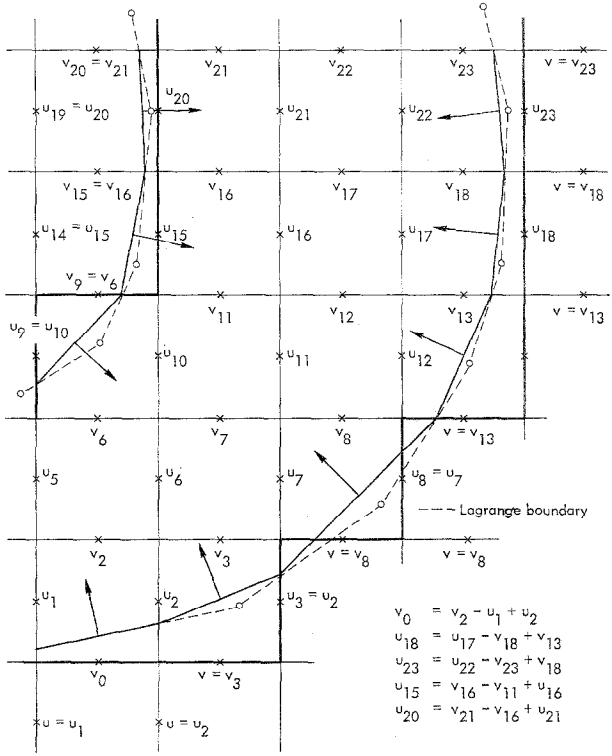

FIG. 3. Determination of mesh velocities on the exterior sides of Eulerian boundary cells and assignment of boundary segment normals.

shows that instead of adjusting the pressure proportional to the divergence or net flux out of a cell one adjusts it proportional to the flux across the boundary measured relative to coordinates fixed in the boundary. If liquid is flowing across the boundary the pressure will be increased until the outflow stops. Conversely if liquid is tending to separate from the boundary the pressure will decrease until the liquid flows tangent to the boundary. Flow separation is of course physically possible because negative pressures do not exist in a liquid. Thus if one assigns a physical meaning to the pressure along a portion of the boundary such as specifying the pressure on a free surface then cell pressures should not drop below the vapor pressure of the liquid. One can take this into account roughly by specifying that $P_{k,l}^{i+1}$ be set equal to the vapor pressure whenver Eq. (9) produces a lower or negative pressure. Supercavitating flows are then possible [5].

Velocities at the exterior sides of the Eulerian boundary cells and other exterior points are necessary in the area weighting formula, and must be recomputed during each iteration sweep. These velocity components are determined in the same way as those on the open sides of free surface cells in the MAC method. In Fig. 3 representative sections of boundary are shown in more detail. The original Lagrange boundaries are indicated by dotted lines, and the resulting boundary segments and normals are shown. Heavy dark lines outline the outer edges of the boundary cells. The values of the velocity components at the edges and outside the Eulerian boundary, where necessary are given, in terms of their interior

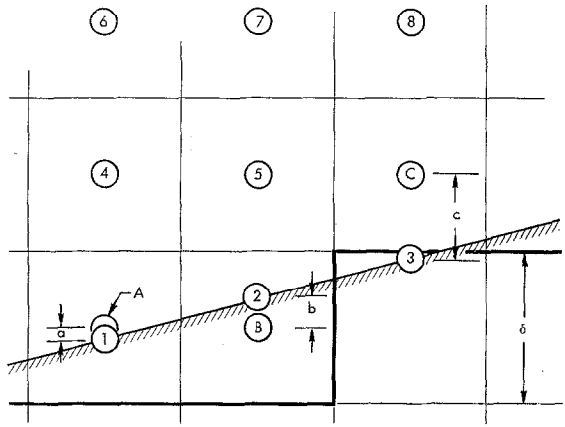

$$P_A = (a P_4 + \delta P_1)/(a + \delta)$$
$$P_B = P_2 + b(P_2 - P_5)/(\delta - b)$$
$$P_C = (c P_8 + \delta P_3)/(c + \delta)$$

FIG. 4. Pressure interpolating scheme.

neighbors for the two-dimensional plane case. In three dimensions with axial symmetry radius factors would be necessary to preserve continuity.

In addition to calculating new cell pressures during each cycle of iteration one must also recalculate the velocity components. During iteration the sum of the old velocity component at time $n\Delta t$, the advection and the viscous terms are stored in $\eta^n_{k+\frac{1}{2},l}$ and $\xi^n_{k,l+\frac{1}{2}}$ which need to be computed only once. Changes in the new cell velocity iterates then depend only on changes in the gradient of the pressure iterates. In the MAC formulation pressure gradients across free surface-full cell boundaries were calculated based on pressures located at the cell centers, though the actual free surface might be anywhere in a cell. However, improved accuracy can be obtained by placing the pressures at the location of the free surface instead of the cell center [2].

In the context of ABMAC this means that if one assigns the location of the boundary pressure to the center of the cell one should extrapolate to get the pres-

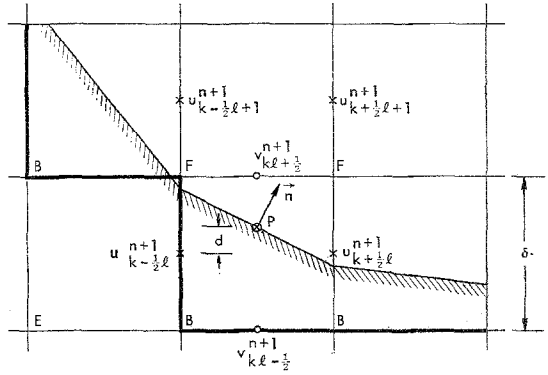

$$u_p^{n+1} = \tfrac{1}{2}\tfrac{d}{\delta}\left(u^{n+1}_{k+\frac{1}{2}\ell+1} + u^{n+1}_{k-\frac{1}{2}\ell+1}\right) + \tfrac{1}{2}\left(1-\tfrac{d}{\delta}\right)\left(u^{n+1}_{k+\frac{1}{2}\ell} + u^{n+1}_{k-\frac{1}{2}\ell}\right)$$

$$v_p^{n+1} = \left(\tfrac{1}{2}+\tfrac{d}{\delta}\right) v^{n+1}_{k\ell+\frac{1}{2}} + \left(\tfrac{1}{2}-\tfrac{d}{\delta}\right) v^{n+1}_{k\ell-\frac{1}{2}}$$

$$u^{n+1}_{k+\frac{1}{2}\ell+1} = \eta^n_{k+\frac{1}{2}\ell+1} - \frac{\Delta t}{\rho\delta}\left(P_{k+1\ell+1} - P_{k\ell+1}\right)$$

$$u^{n+1}_{k-\frac{1}{2}\ell+1} = \eta^n_{k-\frac{1}{2}\ell+1} - \frac{\Delta t}{\rho\delta}\left(P_{k\ell+1} - P_{k-1\,\ell+1}\right)$$

$$u^{n+1}_{k-\frac{1}{2}\ell} = u^{n+1}_{k+\frac{1}{2}\ell} = \eta^n_{k+\frac{1}{2}\ell} - \frac{\Delta t}{\rho\delta}\left(P_{k+1\ell} - P_{k\ell}\right)$$

$$v^{n+1}_{k\ell-\frac{1}{2}} = v^{n+1}_{k\ell+\frac{1}{2}} = \xi^n_{k\ell+\frac{1}{2}} - \frac{\Delta t}{\rho\delta}\left(P_{k\ell+1} - P_{k\ell}\right)$$

$$v_p^{n+1} = m\,u_p^{n+1} \qquad m = \text{Boundary slope at point p}$$

$$\vec{V}_b \equiv 0$$

FIG. 5. First example of the derivation of an explicit boundary condition.

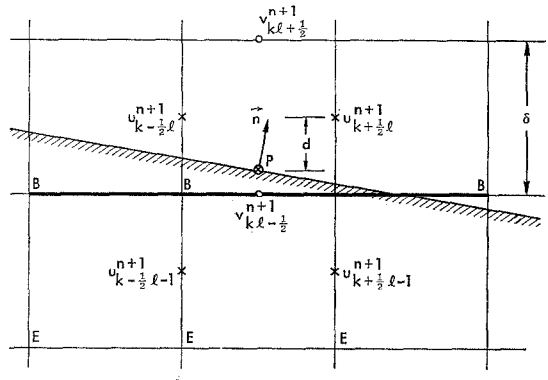

$$u_p^{n+1} = \tfrac{1}{2}\left(1-\frac{d}{\delta}\right)\left(u^{n+1}_{k+\frac{1}{2}\ell} + u^{n+1}_{k-\frac{1}{2}\ell}\right) + \tfrac{1}{2}\frac{d}{\delta}\left(u^{n+1}_{k+\frac{1}{2}\ell-1} + u^{n+1}_{k-\frac{1}{2}\ell-1}\right)$$

$$v_p^{n+1} = \left(\tfrac{1}{2}+\frac{d}{\delta}\right)v^{n+1}_{k\ell-\frac{1}{2}} + \left(\tfrac{1}{2}-\frac{d}{\delta}\right)v^{n+1}_{k\ell+\frac{1}{2}}$$

$$u^{n+1}_{k+\frac{1}{2}\ell-1} = u^{n+1}_{k+\frac{1}{2}\ell} = \eta^{n}_{k+\frac{1}{2}\ell} - \frac{\Delta t}{\rho\delta}\left(P_{k+1\ell} - P_{k\ell}\right)$$

$$u^{n+1}_{k-\frac{1}{2}\ell-1} = u^{n+1}_{k-\frac{1}{2}\ell} = \eta^{n}_{k-\frac{1}{2}\ell} - \frac{\Delta t}{\rho\delta}\left(P_{k\ell} - P_{k-1\ell}\right)$$

$$v^{n+1}_{k\ell+\frac{1}{2}} = \xi^{n}_{k\ell+\frac{1}{2}} - \frac{\Delta t}{\rho\delta}\left(P_{k\ell+1} - P_{k\ell}\right)$$

$$v^{n+1}_{k\ell-\frac{1}{2}} = v^{n+1}_{k\ell+\frac{1}{2}} + u^{n+1}_{k+\frac{1}{2}\ell} - u^{n+1}_{k-\frac{1}{2}\ell}$$

$$v_p^{n+1} = m\,u_p^{n+1} \qquad m = \text{Boundary slope at point p}$$

$$\vec{V}_b = 0$$

FIG. 6. Second example of the derivation of an explicit boundary condition.

sure at the boundary, or alternatively if one assigns the pressure to the boundary point one should interpolate a cell centered pressure to use in the momentum equation. Figure 4 illustrates linear interpolation for the latter method.

A real advantage of the simultaneous iteration method and Eq. (9) is that it gives a simple automatic way of including complicated boundary conditions. One could of course iterate only on the pressure in an explicit form of Poisson's equation as in the MAC method; however, to do this one would have to write down explicit boundary conditions such that the flow would move tangent to the boundary. It can be done but appears to be a formidable task to accomplish with generality because there are so many possible special cases depending on the shape and orientation of the boundary.

To illustrate equivalent explicit forms of the boundary condition, the stationary cases shown in Fig. 5 and 6 have been worked out. Substitution of the expressions for the velocity components into the interpolating formulas for the midpoint

velocity components and in turn substituting the resulting expressions into the boundary condition $v_p^{n+1} = mu_p^{n+1}$ yields for the example in Fig. 5

$$\left(m - 1 - \frac{md}{\delta}\right) P_{k,l} + P_{k,l+1} - \frac{md}{2\delta} P_{k+1,l+1} + \frac{md}{2\delta} P_{k-1,l+1} - m\left(1 - \frac{d}{\delta}\right) P_{k+1,l}$$
$$= \frac{\rho\delta}{\Delta t}\left[\xi^n_{k,l+\frac{1}{2}} - \frac{md}{2\delta}\left(\eta^n_{k+\frac{1}{2},l+1} + \eta^n_{k-\frac{1}{2},l+1}\right) - m\left(1 - \frac{d}{\delta}\right)\eta^n_{k+\frac{1}{2},l}\right], \tag{10}$$

and for the case shown in Fig. 6

$$\frac{\rho\delta}{\Delta t}\left[\xi^n_{k,l+\frac{1}{2}} + \left(\frac{1}{2} + \frac{d}{\delta} - \frac{m}{2}\right)\eta^n_{k+\frac{1}{2},l} - \left(\frac{1}{2} + \frac{d}{\delta} + \frac{m}{2}\right)\eta^n_{k-\frac{1}{2},l}\right]$$
$$= -2\left(1 + \frac{d}{\delta}\right) P_{k,l} + \left(\frac{1}{2} + \frac{d}{\delta} + \frac{m}{2}\right) P_{k-1,l} + \left(\frac{1}{2} + \frac{d}{\delta} - \frac{m}{2}\right) P_{k+1,l} + P_{k,l+1}. \tag{11}$$

Note that advection terms are computed only at the interior sides of boundary cells. In these formulas the pressure is assumed to be located at the center of the boundary cell, so that one would have to extrapolate to get the pressure at the boundary point. Equations (10) and (11) illustrate the actual type of boundary conditions being used. The presence of the variable coefficients multiplying the pressures and the variable number of cells connected with a given boundary condition generally slows down any iterative method of solution so that there is a price to be paid for the convenience and generality of the method.

This modification of the MAC free surface method to the calculation of curved moving wall boundaries illustrates the roughness of the original free surface treatment, i.e., no attempt is made to use the actual width of the open part of a boundary cell side in computing the advection terms or in calculating the divergence, yet fairly good results are obtained when test comparisons with known solutions are made. Perhaps one reason the method works is that incompressible flow fields almost always vary smoothly and slowly so that one can extrapolate to get the velocity at free surface points without having to do elaborate momentum flux calculations. However there is certainly room for refinement if one wishes to expend the effort [8].

Marker Particles and Free Surfaces

The marker particles do not perform any function in ABMAC calculations other than to indicate the position of any free surfaces that may be present. It is likely that in problems containing curved walls or flexible boundaries there will

be no physical free surfaces. In these cases there is no reason why one need include the marker particles. In fact, considerable machine time may be saved by eliminating them. However, if free surfaces are present the marker particles are necessary to tell when liquid enters interior and boundary cells. The marker particles, assuming average densities, specify the fluid configuration with an uncertainty much less than the Eulerian mesh width. Because of this some finer critera other than just the knowledge that a boundary cell contains particles is necessary. We require in addition that

$$(\mathbf{X}_p - \mathbf{X}_n) \cdot \mathbf{n} < \epsilon\delta, \tag{12}$$

where $\mathbf{X}_p$ is the particle position, $\mathbf{X}_n$ is the position of the midpoint of the boundary normal, $\mathbf{n}$ is the boundary normal, and ϵ is some fraction of the cell width δ, typically 1/4. Thus, we do not begin computing a pressure in boundary cells until the particles come within $\epsilon\delta$ of the boundary segment.

When free surfaces are present we also need to know how to treat cells containing the intersection of curved wall boundaries and free surfaces. The pressure at the intersection point should be equal to the ambient pressure, but because the pressure is defined only on the Eulerian net, it is sometimes not possible to zero the flux at the boundary consistent with vanishing divergence without introducing a pressure. This happens when the angle between the free surface and the boundary is small and the liquid is colliding with a wall producing a jet on a scale too fine to be resolved by the Eulerian mesh. We define an intersection cell to be one that contains liquid and has one or more empty interior or pressure surface neighbors, and one or more exterior neighbors. When this definition is satisfied, the pressure is set equal to ambient pressure and the velocities are adjusted directly. In most circumstances the liquid in the cell will be part of a much larger mass. When there are one or two liquid neighbors, the velocity components at the sides in contact with the liquid are preserved, and those at the open and boundary sides adjusted to make the velocity tangent at the boundary consistent with vanishing divergence. In the case of one liquid neighbor, the velocities at the opposite cell sides are assumed equal, and the component with both sides open or boundary is adjusted. In either case the flux at the boundary is a linear function of a single variable, and the zero is easily found. If the velocity at the boundary is initially directed away from the boundary, nothing need be done. The remaining possibility is that there are no liquid neighbors, as happens when a small isolated element strikes the boundary. In this case we set the component of the particle velocity normal to the boundary equal to zero, and preserve the tangential component. If a gravitational force is present we accelerate the particle velocities by the component of the gravitational vector tangent to the boundary.

Stability Limits on the Time Step

There are three restrictions on the size of the time step, Δt. First, it must not be greater than $\delta^2/4\nu$, where δ is the smallest mesh size and ν is the kinematic viscosity. This limit comes from the explicit difference form used to approximate the viscous diffusion terms in the momentum equations (1) and (2). Second, Δt should not be greater than $\epsilon\delta/|\mathbf{V}|_{\max}$, where ϵ is the boundary sensing parameter in Eq. (12) and $|\mathbf{V}|_{\max}$ is the maximum magnitude of the velocity. This restriction prevents particles from moving outside the boundary during the cycle in which liquid first contacts the boundary. Finally, Δt must not exceed the stability limit imposed by the choice of difference scheme for the advection terms.

When backward differencing is used in the advection terms Δt must not exceed $\delta/|\mathbf{V}|_{\max}$. When centered differencing is used there is no value of Δt which will guarantee stability. However, by adding a small amount of viscosity it is possible to damp out instabilities that would otherwise develop [9]. A truncation error analysis shows that one should choose ν so that

$$\nu > \frac{1}{2}\Delta t\,|V|^2_{\max} + \frac{1}{2}\delta^2\left|\frac{\partial u}{\partial x}\right|_{\max}. \tag{13}$$

One should note that Δt appears in the expression for the limit on the size of the relaxation parameter $\Delta\tau$. Therefore when otpimizing the calculation by calculating a new Δt at the end of each cycle, based on the current velocity field, one must also recalculate the relaxation parameter.

Inflow and Outflow Boundary Conditions

An inflow boundary is easily included if one is content with uniform inflow velocity directed perpendicular to the Eulerian mesh boundary. One simply specifies that the normal components of the velocity along the boundary be set to the desired inflow velocity. For example, if one needs an inflow boundary along the radial line $Z = Z_{k,l-\frac{1}{2}}$; $l = 1$; all k, corresponding to the bottom edge of the mesh, one would set $v_{k,l-\frac{1}{2}} = v_{in}$; $l = 1$; all k.

An outflow boundary is generally much more difficult to prescribe. One reason is that the physical flow in the region covered by the mesh depends upon the downstream motion outside the mesh. One way to treat an outflow is to make the mesh big enough so that the flow is essentially uniform by the time it reaches the boundary; then one may specify that the derivatives of the velocity components normal to the mesh boundary be zero. For example, if the radial line $Z = Z_{k,l-\frac{1}{2}}$; $l = 1$; all k, is an outflow boundary one would specify $v_{k,l-\frac{1}{2}} = v_{k,l+\frac{1}{2}}$; $l = 1$; all k.

If the liquid is streaming at an angle to the boundary one also needs to specify a virtual u component lying just outside the mesh so that the u component advection will be calculated correctly when using the centered difference scheme. One would set $u_{k,l-1} = u_{k,l}$; $l = 1$; all k.

This type of outflow boundary condition was used successfully in the test problems shown in Figs. 8 and 11; however difficulties may arise when the liquid is bounded everywhere by walls and there are no free surfaces. In that case there are an infinite number of solutions for the pressure field differing only by arbitrary additive constants. In these circumstances the iterative solution method may never converge unless one specifies the pressure at some point in the flow. One possibility is to pin the pressure at an outflow boundary; for example at the radial line

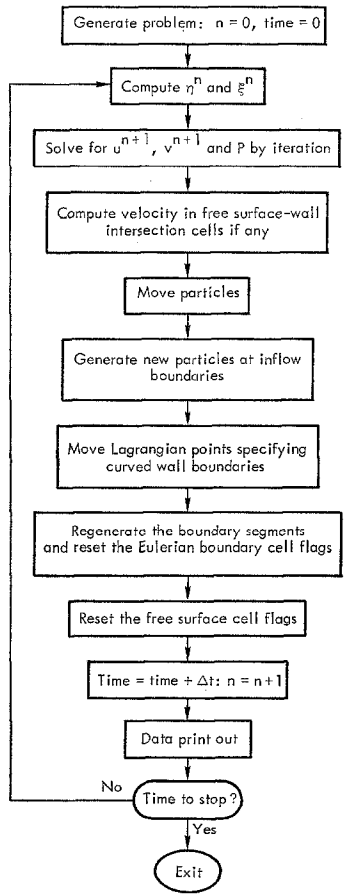

FIG. 7. Flow Chart of the ABMAC program.

$Z = Z_{k,l-\frac{1}{2}}$; $l = 1$; all k one could use (2b) to compute $v_{k,l-\frac{1}{2}}$ with $\xi_{k,l-\frac{1}{2}} = \xi_{k,l+\frac{1}{2}}$ and $P_{k,l-1} = 0$ in a line of virtual cells just outside the bottom edge of the mesh.

Steps in the Calculational Cycle

The first step is to calculate the advection, viscous diffusion, and gravitational acceleration terms in the momentum equations, add them to the old velocities and store the results in η and ξ. Then the simultaneous iteration technique is used to solve for the advanced time velocity components and the pressures. Next, velocities are adjusted in any cells containing the intersection of a free surface and a boundary. The particles are then moved. Note that when inflow and outflow boundaries are present it is necessary to add new particles in inflow cells and to remove particles when they move outside the mesh.

Next the Lagrangian points defining the moving boundary are moved. Then the boundary normals are regenerated and the boundary cell flags are reset. Of course, if the boundaries are stationary the normals and boundary cell flags are

incremented. Data are printed and cathode ray tube pictures are made if desired at the current time or cycle. The cycle of calculation is repeated until one has advanced the solution in time as far as desired. A flow chart of the program is given in Fig. 7.

Test Calculations

One type of test involves comparison of numerically computed asymptotic solutions with those obtained by the hodograph method. One starts the numerical time dependent solution in some configuration far from the steady state and then hopes to see it approach the asymptotic result. Hodograph solutions were worked out for (1) a jet from a nozzle striking a wedge, and (2) a free jet impinging on a plate at arbitrary angle of attack. In the ABMAC calculations the liquid enters from the left, and splashes off the wedge or plate. Inflow and outflow mesh boundaries allow fluid to continue streaming in and out so that eventually a steady flow develops. The free surface configurations and the pressure profiles for these flows are then compared with the hodograph results.

The wedge calculation was done on a 30×40 mesh of square cells with zone size equal to .5. The nozzle width is 2π, the inflow velocity is .763 and the wedge angle is 60°. The plate calculation was done on a 30×30 mesh of square cells

with zone size equal to .25. The plate angle of attack is 84.12° and the free jet width is π. In both cases the free stream velocity is one. The flows are independent of density and no gravitational forces are present. The initial particle density is nine per cell. Centered spatial differencing was used with stabilizing kinematic viscosities of .015 and .05 for the plate and wedge respectively. These viscosities are small in the sense that they are of the same order of magnitude as the coefficients of the diffusion-like truncation errors in the difference equations. In terms of physics they would probably be considered large since the corresponding Reynolds numbers, using the jet width as the characteristic length, are

$$N_p = \frac{1 \times \pi}{.015} \approx 209 \qquad \text{and} \qquad N_w = \frac{1 \times 2\pi}{.05} \approx 126.$$

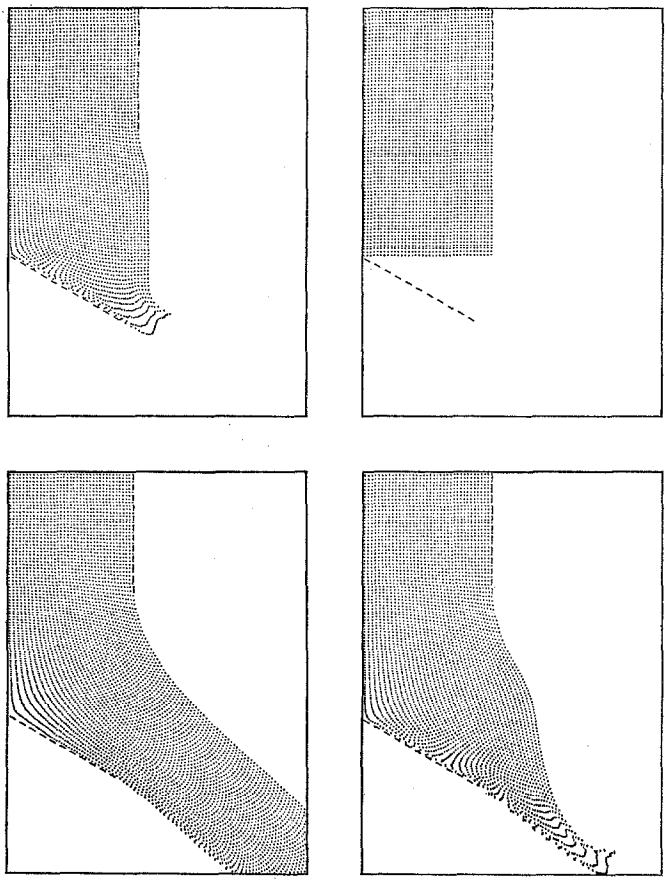

FIG. 8. First test problem: a jet from a nozzle striking a wedge at times 0, 3.55, 7.18, and 24.51.

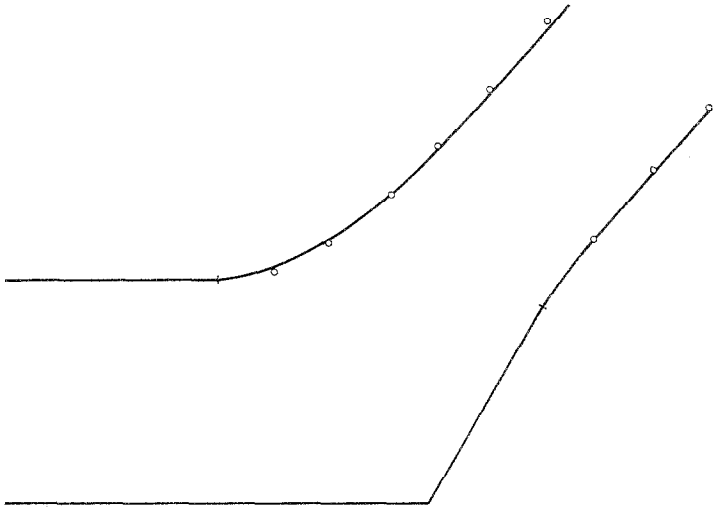

FIG. 9. First test problem: comparison of ABMAC free surface configuration at time 24.51 (data points) with hodograph solution (solid lines).

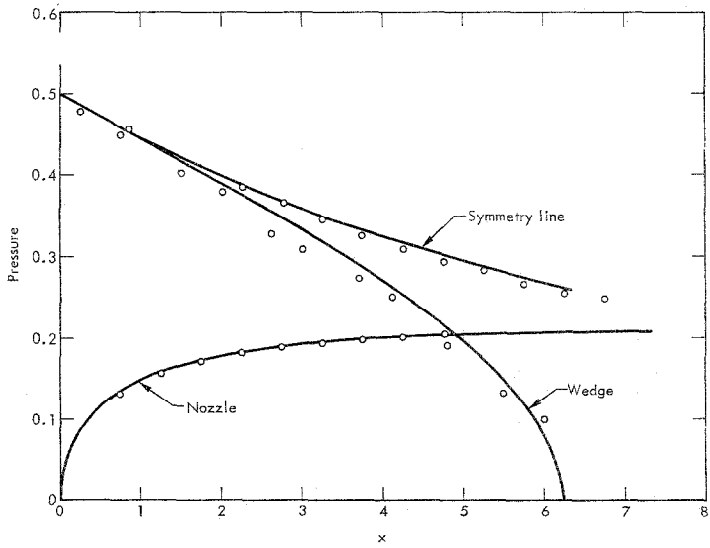

FIG. 10. First test problem: comparison of ABMAC pressures at time 24.51 (data points) with hodograph solution (solid lines).

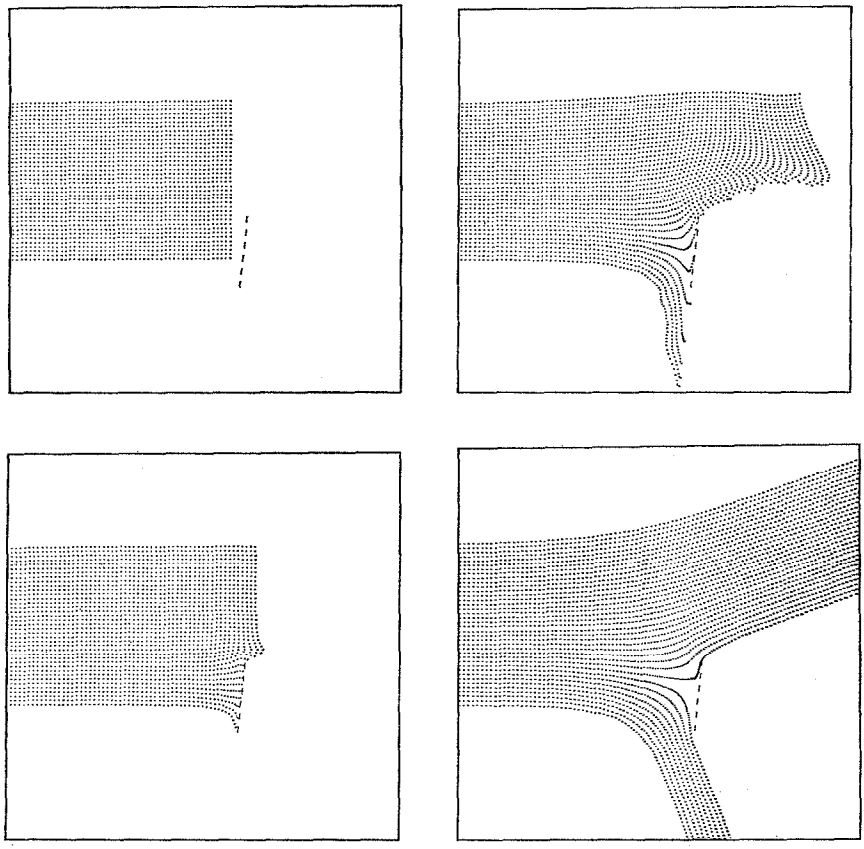

FIG. 11. Second test problem: free jet striking a plate at times 0, .52, 2.25, and 15.46.

The coefficients of the diffusion-like truncation errors are negative for the spatially centered difference scheme, hence the input viscosity coefficient is chosen to insure that it will be larger than the absolute value of any of these coefficients, as indicated in inequality (13). The truncation coefficients are different for each momentum component and depend on the velocity and its gradient, which change with position and time. This means that one cannot assign a physically well defined viscosity to a calculation unless the input viscosity coefficient is much larger than any of the truncation coefficients. Hence the above Reynolds numbers represent only rough estimates since the input viscosity coefficients are only slightly larger than the maximum absolute value of the truncation coefficients. Because the truncation errors are always present one cannot hope to calculate exactly flows with Reynolds numbers above a few hundred with present computing machines.

Nevertheless, finite difference calculations can be used to obtain approximate solutions in many problems characterized by physically large Reynolds numbers as can be seen from the following comparison with the inviscid hodograph theory.

The results of the wedge calculations are shown in Figs. 8, 9, and 10 those for the plate in Figs. 11, 12, and 13. The first figure of each set shows the ABMAC initial configuration, intermediate times when the flow pattern is changing and a very late time when the pattern has essentially become stationary. The next figure in each set shows the comparison between the asymptotic ABMAC free surface position (indicated in the figures by small circles) and those calculated by the hodograph method (indicated by the solid lines). The final figure in each set shows the comparison between pressures calculated by ABMAC and the hodograph method. The ABMAC calculations were done without pressure interpolation in either the free surface or boundary cells. The Eulerian zoning was also fairly rough: the lengths of the wedge and plate are 11 and 6 zones, respectively.

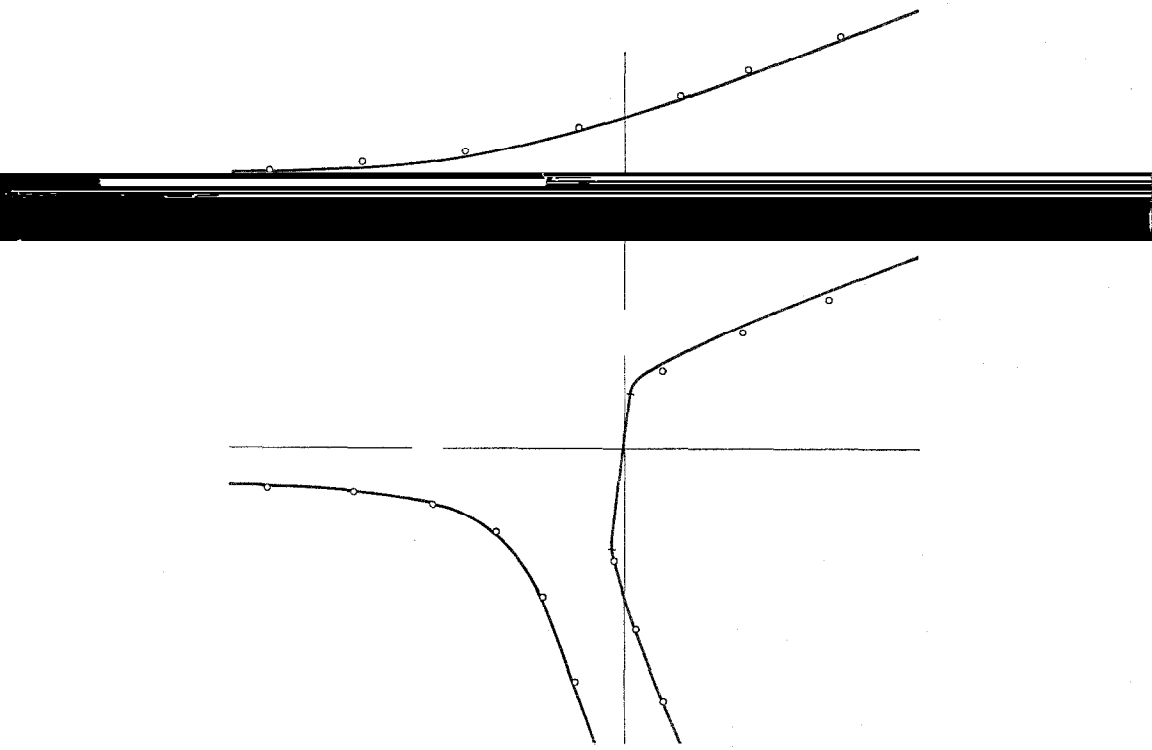

FIG. 12. Second test problem: comparison of ABMAC free surface configuration at time 15.46 (data points) with hodograph solution (solid lines).

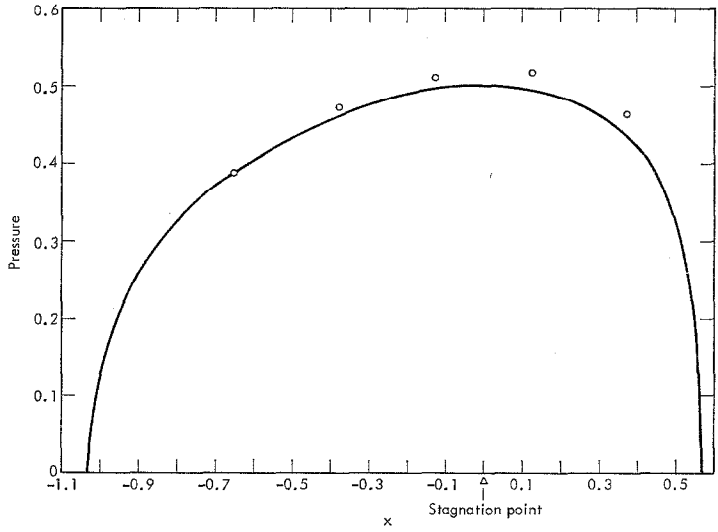

FIG. 13. Second test problem: comparison of ABMAC pressures at time 15.46 (data points) with hodograph solution (solid lines).

EXAMPLES OF FLEXIBLE MOVING BOUNDARIES

As an illustration of the moving boundary capability ABMAC has been used to calculate the motion of a liquid as it is expelled from the top of a cylindrically symmetric heart-shaped flexible bag. The velocity of the ith Lagrangian point defining the bag is taken to be

$$| \mathbf{V}_i | = 5 \cos \frac{\pi}{2} \frac{\theta_i}{\theta_{i_{\max}}} \, e^{-(t-\cdot 5)^2/\cdot 2178} \text{ cm sec}^{-1}.$$

In this formula θ_i is the angle between the axis passing through the closed end of the bag and a ray extending from the origin to the ith Lagrangian boundary point. The velocity of the ith point is taken to be directed along the ray toward the origin at the center of the bag. Thus the point specifying the edge of the bag opening remains fixed while the inward motion of the walls increases to a maximum at the closed end of the bag.

There are 18 axial and 13 radial zones of unit width and the origin is located 10.5 zones from the lower mesh boundary. A viscosity of .1 g cm^{-1} sec^{-1} and density 1.0 gcm^{-3} were used. The radius of the opening at the top is 5 cm. Figure 14 shows the motion of liquid particles and the velocity field as the bag contracts,

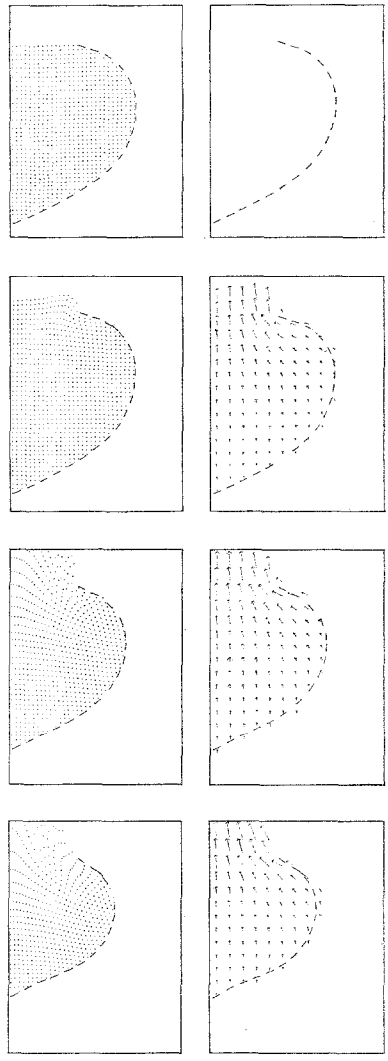

FIG. 14. Flexible wall bag problem: displacements and velocities at times 0., .1, .4, and .7 sec.

expelling the liquid through the hole in the top. With this particular geometry and bag motion the maximum jet velocity attained on the axis was 36 cm sec^{-1} and the pressure reached a peak of 670 dyne cm^{-2} in the center of the bag.

A second example shows the effect of ground motion in generating a water column and wave. Initially a layer of water 2 ft thick lies at rest on the ground surface.

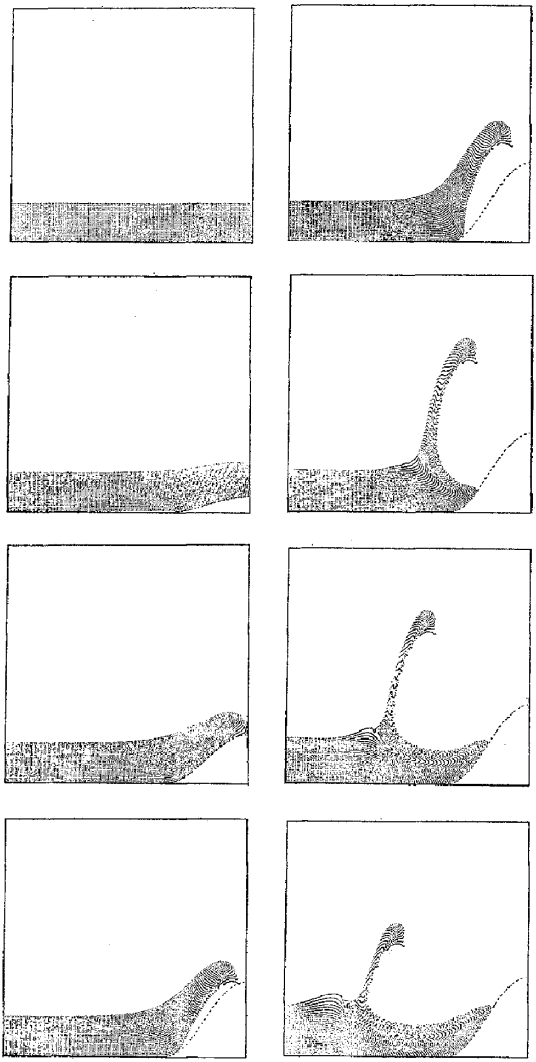

FIG. 15. Water wave problem: liquid configuration at times 0, .090, .147, .210, .286, .551, .855, and 1.044 sec.

The velocity of the ground is given by

$$|V| = \begin{cases} \frac{30}{4}\left[1+\cos\left(\frac{\pi x}{4}\right)\right]\left[1-\cos\left(\frac{2\pi t}{.3}\right)\right] \text{ ft sec}^{-1} & -4 \leqslant x \leqslant 0 \text{ ft} \\ & 0 \leqslant t \leqslant .3 \text{ sec} \\ 0 \quad -4 \leqslant x \leqslant 0 \quad .3 < t \\ 0 \quad x \leqslant -4. \quad 0 \leqslant t \end{cases}$$

and is directed vertically. Thus a mound 4 ft high is formed in a time of .3 sec and the maximum velocity attained is 30 ft sec^{-1}. Figure 15 shows the sequence of events.

As the mound forms it lifts and accelerates the water layer resting on it. At time .15 sec. the ground surface begins to decelerate and the water layer separates from the mound. Its momentum carries it upwards in an arc so that a vertical column of water forms. This column continues moving outwards while collapsing into an outward moving wave. At the same time water sloshes back up the sides of the mound. The calculation was done in plane geometry on a 60×60 mesh with zone width .2 ft and gravitational acceleration 32 sec^{-2}. In this example the vapor pressure and the ambient pressure were set to zero.

REFERENCES

1. F. H. HARLOW AND J. E. WELCH, *Phys. Fluids* **8** (1965), 2182; F. H. HARLOW, J. E. WELCH, J. P. SHANNON, AND B. J. DALY, Los Alamos Scientific Laboratory Report, LA-3425 (1965).
2. R. K.-C. CHAN AND R. L. STREET, *J. Comp. Phys.* **6** (1970), 68.
3. F. H. HARLOW AND J. E. WELCH, *Phys. Fluids* **9** (1966), 842.
4. F. H. HARLOW AND J. P. SHANNON, *J. Appl. Phys.* **38** (1967), 3855.
5. J. A. VIECELLI, *J. Comp. Phys.* **4** (1969), 543.
6. A. J. CHORIN, *Math. Comp.* **22** (1968), 745.
7. J. VON NEUMANN AND R. D. RICHTMYER, *J. Appl. Phys.* **21** (1950), 232.
8. C. W. HIRT AND J. P. SHANNON, *J. Comp. Phys.* **2** (1968), 403.
9. C. W. HIRT, *J. Comp. Phys.* **2** (1968), 339.